

Communication

# Negative Differential Resistance and Long-Lived Changes in the Electrical Conductivity of Carbon Composites Induced by Electrothermal Effects

Wrida Ahmed <sup>1</sup>, Lotfi Chouiref <sup>1</sup>, Hassen Dahman <sup>1</sup>, Lassaad El Mir <sup>1</sup>  and Henrique L. Gomes <sup>2,\*</sup> 

<sup>1</sup> Laboratory of Physics of Materials and Nanomaterials Applied at Environment (LaPhyMNE), Faculty of Sciences in Gabes, Gabes University, Gabes 6072, Tunisia

<sup>2</sup> Instituto de Telecomunicações, Departamento de Engenharia Eletrotécnica e de Computadores, Universidade de Coimbra, 3030-290 Coimbra, Portugal

\* Correspondence: hgomes@uc.pt

**Featured Application:** Non-linear electronic devices and emulation of synapse like behavior.

**Abstract:** In this study, the negative differential resistance (NDR) phenomenon in two-terminal devices composed of pyrogallol-formaldehyde/ZrO<sub>2</sub> composite materials is investigated. It is demonstrated that the NDR is caused by electrothermal effects, which can be observed through the dependence of the NDR on both voltage and temperature. Additionally, it is showed that the NDR peak current and peak/valley voltages can be effectively modulated using electrical pulses that produce mild Joule heating. This modulation arises from the formation of a conductive metastable state, which decays to equilibrium according to power law kinetics. It is suggested that this metastable state is generated through a reversible structural rearrangement induced by heat. The ability to electronically tune the NDR characteristics of carbon composites may have potential applications in electronically controlled oscillators and neuromorphic circuits.

**Keywords:** negative differential resistance; threshold switching; carbon composites; Joule heating



**Citation:** Ahmed, W.; Chouiref, L.; Dahman, H.; El Mir, L.; Gomes, H.L. Negative Differential Resistance and Long-Lived Changes in the Electrical Conductivity of Carbon Composites Induced by Electrothermal Effects. *Appl. Sci.* **2023**, *13*, 1069. <https://doi.org/10.3390/app13021069>

Academic Editor: Vardan Galstyan

Received: 21 November 2022

Revised: 5 January 2023

Accepted: 10 January 2023

Published: 13 January 2023



**Copyright:** © 2023 by the authors. Licensee MDPI, Basel, Switzerland. This article is an open access article distributed under the terms and conditions of the Creative Commons Attribution (CC BY) license (<https://creativecommons.org/licenses/by/4.0/>).

## 1. Introduction

Negative differential resistance (NDR) is an electrical property exhibited by certain electronic circuits and components. NDR has a variety of applications, including storage memory, threshold logic devices, oscillators, and even the emulation of biological neuronal dynamics [1–3]. NDR devices have been realized in a large variety of materials, and several corresponding physical mechanisms have been proposed to explain NDR behavior [4–8]. In the context of this study, the relevant mechanism is self-heating effects [1]. NDR caused by self-heating effects is characterized by an S-shaped I-V characteristic and is often also named current-controlled negative differential resistance. This is because when experimentally recorded, the current in the NDR region is usually controlled by an external resistor. S-shape NDRs have been reported for carbon-based nanostructures [2,3], carbon silica nanocomposites [4], in NbO<sub>2</sub> [5] transition-metal dichalcogenides [6] and in organic-based transistors [7]. The theoretical framework for S-NDR was recently presented in a study by Gibson [1] where it is also claimed that any material where the charge transport is strongly temperature-dependent and the thermal conduction is low enough to generate local Joule heating can exhibit S-NDR. The scaling behavior of devices exhibiting NDR due to electrothermal effects was addressed by Goodwill et al. [8] and a physics-based compact model of the NDR was proposed in a recent review [9]. A more general model, known as the field-triggered thermal runaway (FTTR) model, has been proposed to explain the NDR observed in NbO<sub>2</sub> [10]. This model assumes that the NDR is caused by a combination of an electric-field-based increase in conductivity and Joule heating. A study by Shual

Li et al. presents a detailed model of current-controlled negative differential resistance (NDR) in NbO<sub>x</sub>-based devices and explains a wide range of discrete and compound NDR characteristics observed in these devices [11].

One important characteristic of devices with NDR in their I-V curve is the ability to control the magnitude of the NDR region. For instance, being able to adjust the peak current and the peak/valley voltage ratio allows for the control of oscillation conditions and the power consumption of oscillator circuits. However, tuning the NDR remains a challenge. So far, only transistor devices have shown this potential. For example, ambipolar transistors made of black phosphorus can modulate the NDR by altering the charge type through the inversion of the gate voltage polarity [12]. Double-gate transistors made of graphene can also modulate the magnitude of the NDR by changing the tunneling current through the application of a gate voltage [13]. Modulation of the NDR was also reported in black phosphorus and molybdenum disulfide heterostructures [14].

The main contribution of this study is the demonstration of a simple two-terminal device with the ability to electrically adjust the magnitude of the NDR. The device consists of a pyrogallol-formaldehyde/ZrO<sub>2</sub> composite carbon composite material sandwiched between two silver electrodes, and the magnitude of the NDR can be changed by an order of magnitude when subjected to an electrical current that produces mild Joule heating. The NDR adjustment is caused by an electrothermal effect that generates a metastable change in the electrical conductance of the sample. The metastable state relaxes to equilibrium over a period of approximately 20 h and is fully reversible, with a relaxation process following power-law kinetics. The slow decay of the metastable state allows for the electrical adjustment of the NDR magnitude on a time scale of seconds or minutes, depending on the desired NDR magnitude. To the best of our knowledge, this is the first report of an electrical adjustment of NDR properties using a two-terminal device.

This paper starts by presenting the basic I-V characteristics, including the S-shaped NDR behavior and its agreement with a Joule heating effect. Experimental evidence for the existence of a metastable resistive state induced by Joule heating is also provided. The time scale of the heat-induced state is quantified and discussed in relation to the structural relaxation of the material or the heat-induced diffusion of atmospheric species, such as oxygen and water trapped in the porous structure of the carbon composite.

## 2. Materials and Methods

The pyrogallol-formaldehyde/ZrO<sub>2</sub> (PF/ZrO<sub>2</sub>) composite was synthesized using a simple sol-gel method, which is cost-effective, environmentally friendly, and time-efficient, as well as allowing for the production of materials with a high specific surface area and porosity. In this study, zirconium acetate (C<sub>8</sub>H<sub>12</sub>O<sub>8</sub>Zr; Sigma, St. Louis, MO, USA), a solution in dilute acetic acid, was used as a zirconium source for the synthesis of ZrO<sub>2</sub> nanoparticles. Pyrogallol (P) (C<sub>6</sub>H<sub>3</sub>(OH)<sub>3</sub>; 97%; Fisher Scientific, Waltham, MA, USA) and formaldehyde (F) (CH<sub>2</sub>O; 99%; Biopharm, Iselin, NJ, USA) were used to form the PF matrix. Distilled water (DW) was used as a solvent and picric acid (C<sub>6</sub>H<sub>3</sub>N<sub>3</sub>O<sub>7</sub>; 99%; Scharlau, Barcelona, Spain) was added as a catalyst (C) to promote the gelatinization of the matrix. All the reagents and solvents were analytical-grade and used as received without further purification. In the first step, zirconium oxide (ZrO<sub>2</sub>) aerogel was prepared by a sol-gel method based on the typical synthesis process as described by El Mir et al. [15,16]. The molar ratio of P/F and P/DW were set as 1/3 and 1/6. The weight of ZrO<sub>2</sub> added was 5 wt.%. Subsequently, the wet gel was dried in a humid atmosphere at room temperature for two weeks. Then, the samples were placed into an incubator for drying at 150 °C, with a heating rate of 10 °C/24 h. Finally, the xerogels were treated in a tubular furnace with a heating rate of 5 °C/min under an inert atmosphere (pyrolysis). The furnace held the desired temperature for 2 h to obtain the nanocomposite PF/ZrO<sub>2</sub>. For the samples reported in this study, the pyrolysis temperature was 600 °C. The samples were prepared from the beginning into polypropylene molds to have a cylindrical shape. The samples were completed via two electrical contacts in both faces using conductive silver paint.

The contacts had an active area of  $0.02 \text{ cm}^2$  and samples with a thickness from  $0.19 \text{ cm}$  to  $0.075 \text{ cm}$  were used.

The crystallographic structure of the samples was obtained via X-ray diffraction (XRD) in a Bruker D8 Advance X-ray diffractometer using  $\text{CuK}\alpha$  ( $\lambda = 1.540598 \text{ \AA}$ ) radiation. The morphologies of the obtained nanocomposite were performed via field emission scanning electron microscopy using a LYRA3 TESCAN equipped with an electron-dispersive X-ray (EDX). A detailed morphological and structural characterization of the PF/ $\text{ZrO}_2$  samples is provided in our previous work [17].

Scanning electron microscopy (SEM) images of the PF/ $\text{ZrO}_2$  composite are shown in Figure 1a, and the corresponding X-ray diffraction (XRD) diffractograms are depicted in Figure 1b. Current–voltage (I–V) characterization was conducted using a Keithley 487 picoammeter/voltage source (Portland, OR, USA) and an Agilent 4156C semiconductor parameter analyzer (Santa Clara, CA, USA). Temperature-dependent measurements were performed using an Advanced Research Systems liquid helium close cycle (Macungie, PA, USA), covering a temperature range from 80 to 320 K.

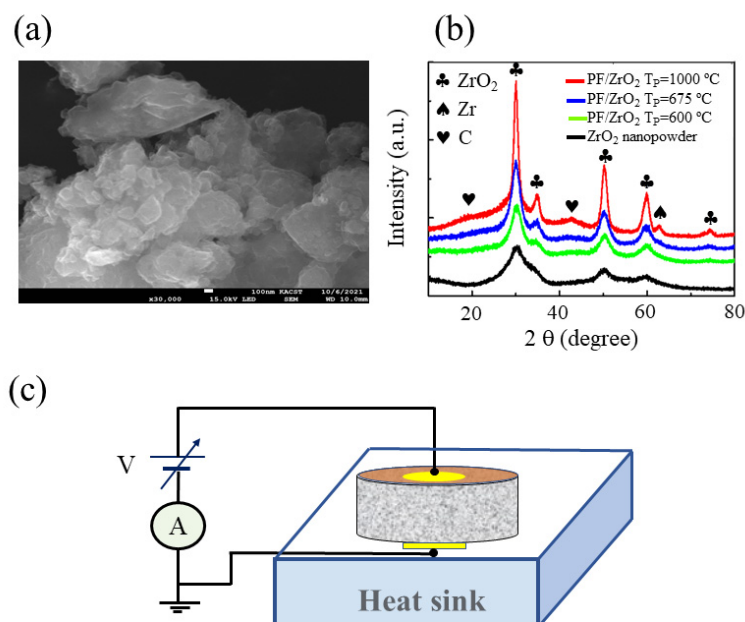


**Figure 1.** (a) SEM photo of a pyrogallol-formaldehyde/ $\text{ZrO}_2$  (PF/ $\text{ZrO}_2$ ) sample. (b) The evolution of the XRD diffractograms with the pyrolysis temperature. (c) Schematic diagram showing the sample mounted in a heat sink and the electrical connections.

The electrical connections of the sample to the measuring circuit are shown in Figure 1c. The samples were mounted on a thick copper holder that acted as a heat sink to dissipate excess heat generated by the Joule effect and prevent thermal runaway. Pulsed I–V measurements were performed by applying voltage steps that lasted 10 milliseconds and were separated in time by 1 s. All electrical measurements were conducted in a vacuum at a pressure of  $10^{-6}$  Torr.

### 3. Results

The porous nature of the films can be clearly seen in the SEM image in Figure 1a. To confirm the incorporation of  $\text{ZrO}_2$  nanoparticles in the host carbon matrix, XRD diffractograms of samples prepared at different pyrolysis temperatures were obtained, as shown in Figure 1b. The XRD patterns of the  $\text{ZrO}_2$  nanoparticles show a series of well-defined peaks at  $2\theta$  values of  $30.1^\circ$ ,  $34.9^\circ$ ,  $50.3^\circ$ , and  $60^\circ$ , which are attributed to the diffractions of the (111), (200), (220), and (311) crystalline planes of the cubic phase according to JCPDS card no. 01-089-9069. The crystallite size of  $\text{ZrO}_2$  nanopowder calculated using Scherrer's

equation is estimated to be equal to 3 nm and increases from 3 to 6 nm when the pyrolysis temperature increases above 600 °C [17].

In our previous studies [15,18], we demonstrated that the incorporation of nanoparticles in the host carbon matrix ameliorated the textural properties and the dielectric behavior of the composite material. We proposed that the nanoparticles played the role of a structuring agent that improved the arrangement of the conduction chains.

The electrical behavior of the pyrogallol-formaldehyde/ZrO<sub>2</sub> (PF/ZrO<sub>2</sub>) composite was investigated using I-V characterization. The devices were sandwich structures (Ag/PF(ZrO<sub>2</sub>)/Ag) using silver paint contacts on both faces. The I-V curves show NDR behavior at high voltages. Figure 2a shows two I-V curves with NDR for two different voltage scan rates. During the forward voltage scan, the current follows a linear behavior that changes to an exponential rise at high voltages. When the voltage scan is reversed, the current continues to increase while the voltage decreases, resulting in an NDR region over a voltage range. The return path has a higher current than the forward path, leading to an anticlockwise hysteresis in the I-V loop.

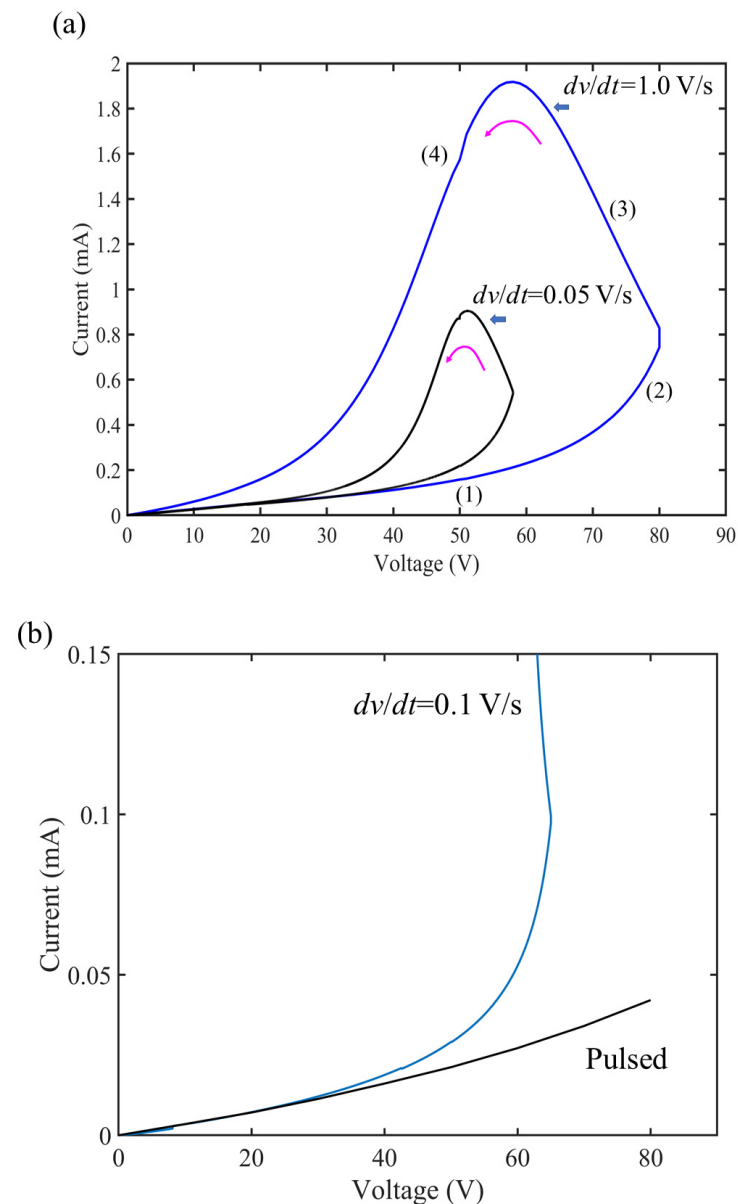


**Figure 2.** (a) Current–voltage characteristics recorded with two different voltage ramp speeds. (b) Comparison between I-V curves measured with a pulsed method and with a voltage ramp method.

I-V curves like those shown in this study have been reported in carbon nanocomposites [18] and other materials such as chalcogenide semiconductors [19] and transition-metal oxides [20].

The voltage scan rate also plays a significant role in the magnitude of NDR, as the duration of applied voltage determines the amount of heat generated through Joule heating. When the device enters the NDR regime, it is necessary to stabilize the I-V curve to prevent thermal runaway, which can damage the device. This can be achieved by decreasing the applied voltage or using a thick device with an intrinsic series resistance that limits the thermal runaway. Thermally activated transport is generally accepted as the cause of negative differential resistance (NDR) in materials such as carbon nanocomposites, chalcogenide semiconductors, and transition metal oxides. This phenomenon occurs due to the low thermal conductivity of the matrix material, and the response time is limited by the heat capacity and generation rate of the device. It is generally agreed that amorphous carbon materials behave as semiconductor materials. Several mechanisms have been proposed to describe the charge transport depending on the temperature range, encompassing the range from an easy thermally activated process obeying the Arrhenius equation to more complex mathematical models, such as variable range hopping. A study by Adrián Bogeat [21] provides a comprehensive review of the models used to interpret the electrical conductivity of amorphous carbon.

The I-V characteristics in Figure 2a do not reflect the sample steady state electrical behavior because Joule heat keeps increasing the internal temperature of the sample. To minimize Joule heating, steady-state I-V characteristics must be recorded upon the application of a train of short (milliseconds long) voltage pulses with increasing amplitude. Furthermore, to prevent cumulative effects due to residual heat, the time between pulses should be at least 1 s long. This method is referred to herein as a pulsed I-V method. Figure 2b compares two I-V curves, one recorded with the pulsed method and the other recorded with a relatively slow voltage ramp speed (0.1 V/s). The remarkable difference between the I-V curves clearly shows the impact of self-heating on the electrical properties of the devices.

The magnitude of the negative differential resistance (NDR) region in the I-V curve can be characterized by the ratio of the peak current to the valley current. This study found that the magnitude of the NDR region can be controlled by adjusting the voltage ramp speed. Additionally, the application of Joule heating pulses can be used to program the magnitude of the NDR. Figure 3 illustrates the programming of the NDR region using voltage ramps. When a series of seven I-V loops were consecutively recorded, the magnitude of the NDR increased by approximately 15 times. It is important to note that between each curve, the sample was left to rest (without applied bias) to dissipate the heat generated by the previous I-V loop.

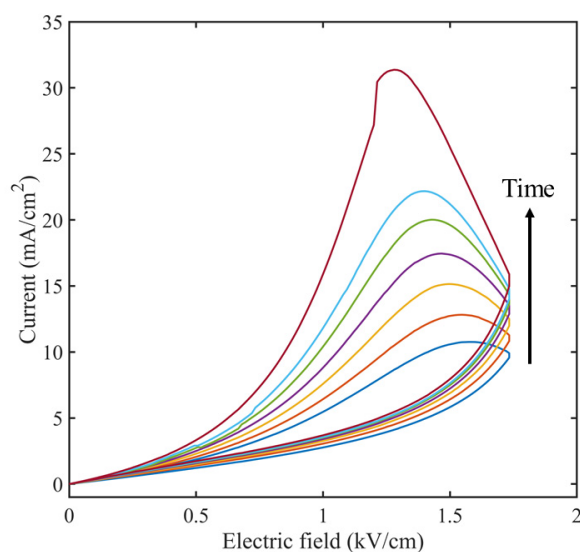


**Figure 3.** The behavior of consecutive I-V loops on the NDR magnitude. The voltage scan rate was 1 V/s. In between each loop, the sample rested for 10 s to dissipate the heat generated by the Joule effect.

The magnitude of NDR causes long-lasting changes in the sample's behavior. As shown in Figure 4, it took around 20 h for the I-V curve to return to its original state after the sample was left to rest. It is difficult to quantify the time constant of this decay using non-steady-state I-V curves (curves recorded with a voltage ramp). However, by measuring the pulsed I-V curve in between each heat cycle, we can gain insight into the underlying physics and quantify the phenomenon. The inset in Figure 4 shows the decay of the current measured at 1 kV/cm plotted on a log–log scale. The decay follows a power law,  $i(t) = (1/t)^\alpha$ , with a small exponent of  $\alpha = 0.03$ , indicating a relatively slow decay.

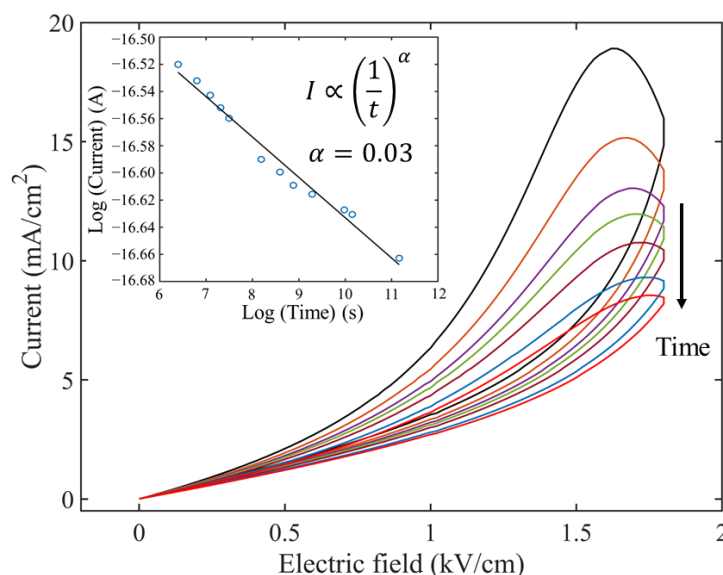


**Figure 4.** Relaxation of the I-V loops when the sample was left resting. The inset shows a log–log plot of the steady state current (measured under a pulsed I-V method) at 1 kV/cm vs. time.

To demonstrate this long-lived memory behavior, the sample was subjected to a series of constant current steps of increasing duration (from 1 s to 10 s). The resulting changes in conductance, caused by Joule heat, were monitored by recording the steady-state I-V curves. To ensure that all the I-V curves were recorded at a constant internal sample temperature, the sample was allowed to rest for 30 s before each pulsed I-V curve measurement to allow the internal heat generated by the pulse to dissipate.

Figure 5 shows the increase in the sample's conductance when well-defined Joule heating pulses were applied ( $I = 20 \mu\text{A}$ ). The inset shows the incremental conductance as a function of pulse duration, with only pulses longer than 4 s causing an increase in conductance. Like the decay described above, these changes also follow a power law with exponent  $\alpha = 0.03$  and were relatively long-lived.

The sample's ability to be temporarily programmed at conductance levels close to one another, combined with the long-lived memory of these changes, has a significant effect on negative differential resistance (NDR) behavior. Even small changes in conductance can lead to a significant increase in current and Joule heating, which drives the NDR properties. The non-linear electrical behavior, with its long-term plasticity under successive excitation, is like that of neural synapses. This suggests that these materials could potentially be explored for use in neuromorphic applications [20].

The current–voltage characteristics of a pyrogallol–formaldehyde sample without ZrO<sub>2</sub> nanoparticles were also studied. These samples, referred to as pristine samples, were found to be less conducting compared to samples doped with 5% of ZrO<sub>2</sub> nanoparticles (see Figure S1). We also observed that ZrO<sub>2</sub> nanoparticles did not directly contribute to the negative differential resistance observed in the I-V curves. As demonstrated in Figure S2, samples prepared without ZrO<sub>2</sub> nanoparticles also exhibited NDR. Furthermore, upon Joule heating, we also observed long-lived relaxation effects on the sample conductivity.

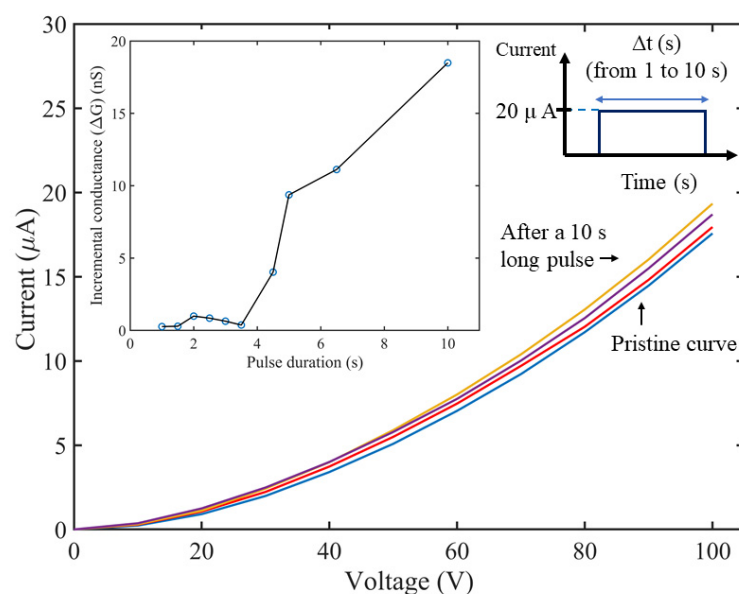


**Figure 5.** Set of I-V curves measured in pulsed mode and programmed with consecutive Joule heating pulses. Applied pulses were at constant current ( $20 \mu\text{A}$ ) and increasing duration. The inset shows the incremental change in conductance as a function of the length of the heating pulse.

#### 4. Discussion and Conclusions

In this study, the non-linear electrical properties of pyrogallol–formaldehyde are investigated. It is shown that the resistance of this material can be reversibly switched using electrical pulses or voltage ramps. The resistance change is believed to be caused by Joule heating, which leads to the formation of a hot conducting filament across the sample.

It is also demonstrated that the  $\text{ZrO}_2$  nanoparticles improve the sample conductivity but do not have a direct role in the NDR properties nor in the metastable changes in sample resistance.

The rise in temperature caused by Joule heating is not expected to be high enough to cause significant changes in the carbon bonds or graphitization. Carbon exists in various forms, including the low-resistivity  $\text{sp}^2$ -dominated graphitic form and the high-resistivity  $\text{sp}^3$ -dominated diamond form. It is known that heating carbon to temperatures above  $600^\circ\text{C}$  under controlled conditions (pyrolysis) can alter the  $\text{sp}^2/\text{sp}^3$  ratio or cluster existing  $\text{sp}^2$  sites, but these changes in carbon bonds result in permanent changes in resistance, which cannot account for the fully reversible changes in resistance reported in this study.

The electric field may also play a role in the observed resistance changes. Previous studies using a scanning tunnelling microscope probe have shown that high electric fields can induce structural changes in amorphous carbon [22]. While the electric field applied to our samples was below  $3 \text{ kV/cm}$ , it is possible that the combination of heat and electric field led to changes in carbon rearrangements. Further research is needed to clarify the role of both heat and electric field, including studies that vary sample thickness and combine electrical measurements with structural techniques.

The samples studied in this research are porous, with a large surface area to volume ratio, and they can absorb atmospheric species such as oxygen and water. Evidence for absorbed water was found in the Fourier transform infrared spectroscopy (FTIR) spectrum of the PF/ $\text{ZrO}_2$  samples [17]. It is expected that surface/bulk effects from the interaction with adsorbates significantly affect the material's conductivity. It is also known that trapped water, behaving as supercritical water, can mediate chemical reactions and affect the electrical conductivity of carbon-based materials [23]. The effects of absorbed water on the electrical conductivity of carbon-based materials are discussed in a comprehensive review by Adrián Barroso Bogeat [21]. We speculate that upon heating, absorbed chemical species may diffuse out from the hot filament to nearby regions, and when the filament

cools down, the chemical species may diffuse back, restoring the original conductivity. However, further work is needed to understand the role of absorbed oxygen and water in the reversible changes in resistance caused by Joule heat.

The fine adjustment of electrical properties makes pyrogallol-formaldehyde/ZrO<sub>2</sub> composites appealing for various electronic devices, including volatile memory devices, devices that mimic the long-term plasticity of biological synapses, threshold switching devices, and oscillator circuits that utilize negative differential resistance properties.

**Supplementary Materials:** The following supporting information can be downloaded at: <https://www.mdpi.com/article/10.3390/app13021069/s1>, Figure S1: Comparison between the electrical conductivity of the pyrogallol-formaldehyde sample with the sample doped with 5% of ZrO<sub>2</sub> nanoparticles. The conductivity was measured for several pyrolysis temperatures. Figure S2: Current-voltage characteristics of a pyrogallol-formaldehyde sample without ZrO<sub>2</sub> nanoparticles. The voltage scan rate was 1 V/s. The sample has an active area of 0.008 cm<sup>2</sup> and a thickness of 0.05 cm.

**Author Contributions:** Conceptualization, H.L.G. and L.E.M.; methodology, H.L.G.; validation, H.L.G., L.E.M. and H.D.; formal analysis, H.L.G. and L.E.M.; investigation, W.A., L.C. and H.D.; resources, H.L.G. and L.E.M.; data curation, H.L.G., W.A. and L.C.; writing—original draft preparation, H.L.G.; writing—review and editing, H.L.G. and L.E.M.; visualization, L.C. and W.A.; supervision, H.L.G. and L.E.M.; project administration, L.E.M.; funding acquisition, L.E.M. All authors have read and agreed to the published version of the manuscript.

**Funding:** This research was funded by the Portuguese Foundation for Science and Technology (FCT/MCTES), through the UIDB/50008/2020 (Instituto de Telecomunicações, IT), through national funds, and when applicable, through co-funded EU funds by FEDER under the PT 2020 Partnership. The research was also funded by the Tunisian Ministry of Higher Education, by Scientific Research through the budget of the Tunisian Laboratories.

**Data Availability Statement:** The data that support the findings of this study are available from the corresponding author upon reasonable request.

**Conflicts of Interest:** The authors declare no conflict of interest.

## References

1. Gibson, G.A. Designing Negative Differential Resistance Devices Based on Self-Heating. *Adv. Funct. Mater.* **2018**, *28*, 1704175. [[CrossRef](#)]
2. Evlashin, S.A.; Tarkhov, M.A.; Chernodubov, D.A.; Inyushkin, A.V.; Pilevsky, A.A.; Dyakonov, P.V.; Pavlov, A.A.; Suetin, N.V.; Akhatov, I.S.; Perebeinos, V. Negative Differential Resistance in Carbon-Based Nanostructures. *Phys. Rev. Appl.* **2021**, *15*, 054057. [[CrossRef](#)]
3. Yu, Y.; Zhao, B.; Goodwill, J.M.; Ma, Y.; Bain, J.A.; Skowronski, M. Electrical and Thermal Dynamics of Self-Oscillations in TaOx-Based Threshold Switching Devices. *ACS Appl. Electron. Mater.* **2020**, *2*, 683–691. [[CrossRef](#)]
4. Gouadria, S.; Najeh, I.; El Mir, L. Carbon-Silica Nanocomposite with Negative Differential Resistance for High Voltage Negatronic Devices: Effect of Silica Concentration. *J. Phys. Chem. Solids* **2017**, *110*, 290–296. [[CrossRef](#)]
5. Slesazek, S.; Mähne, H.; Wylezich, H.; Wachowiak, A.; Radhakrishnan, J.; Ascoli, A.; Tetzlaff, R.; Mikolajick, T. Physical Model of Threshold Switching in NbO<sub>2</sub> Based Memristors. *RSC Adv.* **2015**, *5*, 102318–102322. [[CrossRef](#)]
6. Wang, M.; Wang, C.Y.; Wu, C.; Li, Q.; Pan, C.; Wang, C.; Liang, S.J.; Miao, F. S-Type Negative Differential Resistance in Semiconducting Transition-Metal Dichalcogenides. *Adv. Electron. Mater.* **2019**, *5*, 1800853. [[CrossRef](#)]
7. Klinger, M.P.; Fischer, A.; Kleemann, H.; Leo, K. Non-Linear Self-Heating in Organic Transistors Reaching High Power Densities. *Sci. Rep.* **2018**, *8*, 9806. [[CrossRef](#)]
8. Li, D.; Goodwill, J.M.; Bain, J.A.; Skowronski, M. Scaling Behavior of Oxide-Based Electrothermal Threshold Switching Devices. *Nanoscale* **2017**, *9*, 14139–14148. [[CrossRef](#)]
9. Brown, T.D.; Kumar, S.; Williams, R.S. Physics-Based Compact Modeling of Electro-Thermal Memristors: Negative Differential Resistance, Local Activity, and Non-Local Dynamical Bifurcations. *Appl. Phys. Rev.* **2022**, *9*, 011308. [[CrossRef](#)]
10. Goodwill, J.M.; Ramer, G.; Li, D.; Hoskins, B.D.; Pavlidis, G.; McClelland, J.J.; Centrone, A.; Bain, J.A.; Skowronski, M. Spontaneous Current Constriction in Threshold Switching Devices. *Nat. Commun.* **2019**, *10*, 1628. [[CrossRef](#)]
11. Li, S.; Liu, X.; Nandi, S.K.; Nath, S.K.; Elliman, R.G. Origin of Current-Controlled Negative Differential Resistance Modes and the Emergence of Composite Characteristics with High Complexity. *Adv. Funct. Mater.* **2019**, *29*, 1905060. [[CrossRef](#)]
12. Cheng, R.; Yin, L.; Hu, R.; Liu, H.; Wen, Y.; Liu, C.; He, J. Modulation of Negative Differential Resistance in Black Phosphorus Transistors. *Adv. Mater.* **2021**, *33*, 2008329. [[CrossRef](#)] [[PubMed](#)]

13. Niyat, F.Y.; Hosseini, S.E. A Novel AGNR/h-BN Transistor with Tunable Negative Differential Resistance. *Phys. E Low Dimens. Syst. Nanostruct.* **2020**, *121*, 114110. [[CrossRef](#)]
14. Wu, F.; Tian, H.; Yan, Z.; Ren, J.; Hirtz, T.; Gou, G.; Shen, Y.; Yang, Y.; Ren, T.L. Gate-Tunable Negative Differential Resistance Behaviors in a HBN-Encapsulated BP-MoS<sub>2</sub>Heterojunction. *ACS Appl. Mater. Interfaces* **2021**, *13*, 26161–26169. [[CrossRef](#)]
15. Mansour, N.B.; El Mir, L. Influence of the Nickel Oxide Nanoparticles Content on the Electrical Properties of Carbon/Nickel Nanocomposites. *J. Mater. Sci. Mater. Electron.* **2017**, *28*, 11284–11291. [[CrossRef](#)]
16. El Mir, L.; Kraiem, S.; Bengagi, M.; Elaloui, E.; Ouederni, A.; Alaya, S. Synthesis and Characterization of Electrical Conducting Nanoporous Carbon Structures. *Phys. B Condens. Matter.* **2007**, *395*, 104–110. [[CrossRef](#)]
17. Ahmed, W.; Jeidi, H.; Chouiref, L.; Gomes, H.L.; Dahman, H.; El Mir, L. Threshold Switching Behavior Generated by the in situ Filaments Formation in Carbon Matrix Enriched by Ultra-Small Zirconium Oxide Nanoparticles. *Appl. Phys. A* **2023**, *129*, 60. [[CrossRef](#)]
18. Gouadria, S.; Dahman, H.; Omri, K.; El Mir, L. Negative Differential Resistance in Carbon-Silica Nanocomposites. *Int. J. Nanotechnol.* **2013**, *10*, 597–606. [[CrossRef](#)]
19. Abay, B.; Gürbulak, B.; Yildirim, M.; Efeoğlu, H.; Tüzemen, S.; Yogurtçu, Y.K. Electrothermal Investigation of the Switching Effect in P-Type TlInSe<sub>2</sub>, TlInTe<sub>2</sub> and TlGaTe<sub>2</sub> Chain Chalcogenide Semiconductors. *J. Electron. Mater.* **1996**, *25*, 1054–1059. [[CrossRef](#)]
20. Nune, P.; Mandal, S. TaOxbased Memristor Model and Its Emulator Design for Future Neuromorphic Computing. In Proceedings of the 13th International Conference on Electronics, Computers and Artificial Intelligence, ECAI, Pitesti, Romania, 1–3 July 2021. [[CrossRef](#)]
21. Barroso Bogeat, A. Understanding and Tuning the Electrical Conductivity of Activated Carbon: A State-of-the-Art Review. *Crit. Rev. Solid State Mater. Sci.* **2021**, *46*, 1–37. [[CrossRef](#)]
22. Mercer, T.W.; DiNardo, N.J.; Rothman, J.B.; Siegal, M.P.; Friedmann, T.A.; Martinez-Miranda, L.J. Electron Emission Induced Modifications in Amorphous Tetrahedral Diamondlike Carbon. *Appl. Phys. Lett.* **1998**, *72*, 2244–2246. [[CrossRef](#)]
23. Tayyebi, A.; Akhavan, O.; Lee, B.K.; Outokesh, M. Supercritical Water in Top-down Formation of Tunable-Sized Graphene Quantum Dots Applicable in Effective Photothermal Treatments of Tissues. *Carbon N. Y.* **2018**, *130*, 267–272. [[CrossRef](#)]

**Disclaimer/Publisher's Note:** The statements, opinions and data contained in all publications are solely those of the individual author(s) and contributor(s) and not of MDPI and/or the editor(s). MDPI and/or the editor(s) disclaim responsibility for any injury to people or property resulting from any ideas, methods, instructions or products referred to in the content.